

# XAS spectroelectrochemistry: reliable measurement of X-ray absorption spectra from redox manipulated solutions at room temperature

Stephen P. Best,<sup>a\*</sup> Aviva Levina,<sup>b</sup> Chris Glover,<sup>c</sup> Bernt Johannessen,<sup>c</sup> Peter Kappen<sup>c</sup> and Peter A. Lay<sup>b</sup>

Received 26 January 2016

Accepted 1 April 2016

Edited by R. W. Strange, University of Liverpool, UK

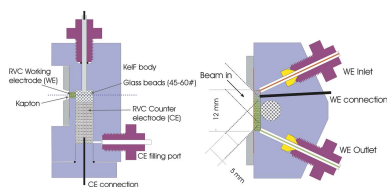
**Keywords:** XAS; XANES; spectroelectrochemistry; metalloproteins; trioxalatoferrate(III).

<sup>a</sup>School of Chemistry, University of Melbourne, Parkville, Melbourne, Victoria 3010, Australia, <sup>b</sup>School of Chemistry, The University of Sydney, Sydney, New South Wales 2006, Australia, and <sup>c</sup>Australian Synchrotron, 800 Blackburn Road, Clayton, Victoria 3168, Australia. \*Correspondence e-mail: spbest@unimelb.edu.au

The design and operation of a low-volume spectroelectrochemical cell for X-ray absorption spectroscopy (XAS) of solutions at room temperature is described. Fluorescence XAS measurements are obtained from samples contained in the void space of a 50  $\mu\text{L}$  reticulated vitreous carbon (sponge) working electrode. Both rapid electro-synthesis and control of the effects of photoreduction are achieved by control over the flow properties of the solution through the working electrode, where a good balance between the rate of consumption of sample and the minimization of decomposition was obtained by pulsing the flow of the solution by 1–2  $\mu\text{L}$  with duty cycle of  $\sim 3$  s while maintaining a small net flow rate (26–100  $\mu\text{L h}^{-1}$ ). The performance of the cell in terms of control of the redox state of the sample and minimization of the effects of photoreduction was demonstrated by XAS measurements of aqueous solutions of the photosensitive  $\text{Fe}^{\text{III}}$  species,  $[\text{Fe}(\text{C}_2\text{O}_4)_3]^{3-}$ , together with that of the electrogenerated  $[\text{Fe}(\text{C}_2\text{O}_4)_3]^{4-}$  product. The current response from the cell during the collection of XAS spectra provides an independent measure of the stability of the sample of the measurement. The suitability of the approach for the study of small volumes of mM concentrations of protein samples was demonstrated by the measurement of the oxidized and electrochemically reduced forms of cytochrome *c*.

## 1. Introduction

Spectroelectrochemical (SEC) techniques have been shown to offer significant benefits for the study of redox active molecules (Kaim & Klein, 2008; Bond & Scholz, 2010). The main value obtained from this strategy comes from the ability to exert a high level of control over the redox form of the sample under spectroscopic investigation. The art of the approach comes from balancing the different advantages and disadvantages presented by the electrochemical and spectroscopic techniques. Similar considerations lie behind the development of *operando* spectroscopy as is increasingly important in the study of catalysis (Wachs, 2003; Weckhuysen, 2003) and batteries (Nakanishi *et al.*, 2014; Permien *et al.*, 2016). It is important to make a distinction between approaches that utilize electro-synthetic methods to generate a sample [that can then be measured *ex situ* with X-ray absorption spectroscopy (XAS)] and those that employ *in situ* spectroscopic interrogation of electrochemically generated compounds. In the former case the state of the electro-generated sample can be validated by independent spectroscopic methods; however, the sample must be maintained in its electro-generated state for the duration of the measurement.



The collection of XAS of sufficient quality for structural analysis presents significant challenges both in terms of the rate of data collection and the additional complications caused by photoreduction. It has been shown that the linking of electrosynthesis and cryogenic stabilization of the electro-generated product can allow the measurement of good quality XAS data from reactive redox generated species (Bondin *et al.*, 2001, 2006a,b; Best & Cheah, 2010; Cheah & Best, 2011).

Several approaches have been reported that allow *in situ* XAS measurements from samples in controlled redox states and these use methodologies that range from bulk electrosynthesis cells (typically of volume 1–10 ml) with large-surface-area electrodes (Dewald *et al.*, 1986; Bae *et al.*, 2001; Levina *et al.*, 2004; Hennig *et al.*, 2005; Milsman *et al.*, 2006; Takao *et al.*, 2010) to channel-flow cells (Wiltshire *et al.*, 2009) and cells optimized for the study of electrode transformations (McBreen *et al.*, 1987; Nakanishi *et al.*, 2014). While bulk electrosynthesis cells have been used to obtain XAS spectra, the long electrosynthesis period (typically >10 min) makes them impracticable for the study of short-lived reactive species, or for samples, such as metalloproteins, that are only available in small quantities. The channel-flow cell of Wiltshire and co-workers presents a narrow cross-section ( $\sim 1 \text{ mm}^2$ ) and a flow rate of  $200 \mu\text{L h}^{-1}$  would correspond to a residence time of the sample of  $\sim 1 \text{ s}$  in a  $50 \mu\text{m}$  focused beam (Wiltshire *et al.*, 2009). However, the suitability of this approach is limited by the comparatively small extent of electrosynthesis able to be obtained under working conditions (5% conversion when using a  $400 \mu\text{m}$ -wide ribbon electrode).

In order to deal with the issues related to reactive compounds and/or those that are only available in small quantities, approaches have been developed that allow electrosynthesis in a cell of dimensions able to be transferred to a cryostat (Yeo *et al.*, 2012). In this case the working electrode (WE) also functions as the XAS sample holder and the electrosynthesized sample is frozen in the WE and the cell transferred to the beamline cryostat. Using this approach the minimum sample volume is of the order of  $200 \mu\text{L}$ . While this represents a significant advance, there are issues associated with the perturbation of the sample as a consequence of cooling to cryogenic temperatures. For transition metals in biological and abiological environments the local structure about the metal can be perturbed directly, through temperature-dependent changes in spin state (Nakamura & Takahashi, 2013; Day *et al.*, 1967; Harris & Loew, 1993; Nihei *et al.*, 2007; Craig *et al.*, 2014; Guionneau, 2014; Beattie, 1988), or indirectly, through changes in protein conformation resulting from the temperature-dependence of the  $\text{p}K_{\text{a}}$  of the amino acid sidechains (Alonso *et al.*, 1991; Hutchens & Yip, 1991; Osheroff *et al.*, 1980). Spin equilibria is often encountered in systems, such as heme proteins, where this can also be related to exchange of the coordinating ligands; for example, the met  $\text{Fe}^{\text{III}}$  forms of heme proteins are often in spin equilibrium at biologically relevant temperatures, with the high-spin aqua form highly favoured, but the EXAFS determined structures at 10 K show low-spin  $\text{Fe}^{\text{III}}$  with bis-his coordination (Levina *et al.*, 2005). Further, the spin state of the metal can be

changed as a result of protein–protein interactions such as the high- to low-spin state change associated with  $\alpha$ -hemoglobin specific binding protein (AHSP) binding to  $\alpha$ -hemoglobin (Feng *et al.*, 2004; Dickson *et al.*, 2013). Therefore, XAS techniques are desirable that will enable the capture of the structures of physiologically relevant spin-states of proteins and to study their interconversions with potential physiological partners.

Even in cases where the structures of metalloproteins under physiological conditions are maintained at low temperatures, photoreduction at modern high-flux beamlines can be so significant that it is still not possible to obtain reliable structures from samples held at 10 K (George *et al.*, 2012; Levina *et al.*, 2005, 2014, 2015). This is a conundrum because the high-flux beamlines are required to obtain high-quality EXAFS from dilute solutions of metalloproteins. The issue of photoreduction is particularly problematic for static solution samples since diffusion allows chemical reactions between the primary photoproducts (usually solvent) and the solute species. Thus, it is important to develop methodologies that take advantage of the high signal-to-noise ratios for XAS measurements made achievable by high-flux beamlines, whilst also mitigating the effects of photoreduction. At the extreme of very high intensity free-electron laser beamlines, jet techniques have been developed to allow XRD measurements in a single X-ray pulse (Johansson *et al.*, 2012; Chapman *et al.*, 2011) but this comes at a cost of sample; the strategy we propose is to obtain measurements from a flowing solution, where control of the flow can both minimize photoreduction and limit the sample requirements for collection of XAS with quality suitable for structural analysis.

In this contribution we describe the design of a low-volume SEC cell for *in situ* XAS where the sample under spectroscopic investigation is in close contact with the WE of the electrochemical cell. Key requirements of the approach are: (i) the redox state of the sample under irradiation is controlled electrochemically; (ii) the volume of sample needed for the collection of high-quality XAS spectra is of the order 100–200  $\mu\text{L}$ ; and (iii) the sample degradation by the X-ray beam can be controlled. The successful operation of the cell is demonstrated by the quality of the XAS spectra collected from solutions of  $\text{K}_3[\text{Fe}(\text{ox})_3]$ , together with that of its electrochemically reduced partner,  $[\text{Fe}(\text{ox})_3]^{4-}$ . The suitability of the approach for the study of metalloproteins is demonstrated by measurement of the oxidized and reduced forms of cytochrome *c* (cyt *c*) that we have studied previously at 10 K (Cheng *et al.*, 1999).

## 2. Experimental

### 2.1. Chemicals and materials

Unless otherwise stated, chemicals were obtained from Sigma-Aldrich and were used without further purification. Horse heart cyt *c* was obtained from Sigma (>95%, cat. No. C2506) and was used without further purification. Samples of

$K_3[Fe(ox)_3]$  were prepared by standard methods (Malati, 1999).

Electrochemical measurements were conducted in the purpose-built cell described in the following section. The cell incorporated a Cypress systems EE009 no leak Ag/AgCl reference electrode (RE) and the WE and counter electrodes (CE) were constructed from reticulated vitreous carbon (500 p.p.i.; Destech Corporation), which had been treated by immersion in concentrated sulfuric acid and thoroughly rinsed with MilliQ water so as to render the surface hydrophilic. Solutions of  $K_3[Fe(ox)_3]$  (5.0 mM) were prepared using MilliQ water with  $K_2SO_4$  (0.2 M) as the supporting electrolyte and solutions of cyt *c* (5.0 mM) contained 10 mM 4,4'-bipyridine to mediate electron transfer in the phosphate-buffered saline (20 mM phosphate, 140 mM NaCl, pH 7.4) (Eddowes & Hill, 1979). All solutions were degassed prior to loading into the gas-tight syringes.

## 2.2. Cell design and operation

Vertical and horizontal sections through the WE compartment of the XAS-SEC cell are shown in Fig. 1. The cell body was constructed from Kelf or glass-filled Teflon with cavities to accommodate the 2 mm × 2 mm × 12 mm WE, the 6 mm-diameter CE and a 2 mm hole for insertion of the RE. The space between the electrodes was packed with glass beads (45–60 mesh; Selby) of a diameter sufficiently large to be excluded from the cavities of the reticulated vitreous carbon (RVC) electrodes. The purpose of the glass beads is to minimize mixing between the solution in the working electrode and the supporting electrolyte. Liquid chromatography fittings were used to seal the 1/16-inch outer-diameter Teflon tubing into the cell. The WE and CE were cut from a sheet of RVC and both electrodes were carefully placed in their respective positions in the XAS-SEC cell and electrical contact was achieved through mechanical contact with platinum wires sealed into the cell body. An O-ring seal ensured an air-tight

seal between the RE and the cell body. A Kapton sheet clamped against the cell block encloses the WE chamber while minimizing the absorption of X-rays. Redox reaction between the dye in the Kapton film and the redox-generated molecules has been observed when conducting reductions using non-aqueous solutions; this issue can be avoided by the use of Teflon-coated Kapton.

During cell operation, exclusion of air was achieved by introduction of the solvent/supporting electrolyte through the CE filling port without the RE sealed in the cell. Atmospheric contamination can be minimized by maintaining a flow of  $N_2$  through the WE inlet and outlet ports. Once the level of the solution was visible in the RE cavity, the flow of solution and gas was stopped and the RE was fixed in place and the solution flow through the CE was restored with the solution drained through the WE inlet and outlet ports. At this point the electrochemical performance of the cell was checked by monitoring the changes in background current with a change of applied potential.

Finally, the flow of solvent/supporting electrolyte was stopped and the inlet and outlet ports of the WE were then connected to their respective matched syringe pumps. At this point the cell was a closed system and the inlet and outlet syringes must be driven synchronously so as to achieve a flow of solution through the cell while minimizing any pressure change. The volume of solution needed to transfer the solution front from the syringe through to the exit of the sample chamber depended on the inner diameter and length of the Teflon tubing. For the experiments described below, 0.02-inch inner diameter Teflon tubing with flange seals were used and ~95  $\mu$ L was required to transfer the solution from the syringe through the Hamilton HV valve to the entry point of the cell. This could be reduced to ~26  $\mu$ L by the use of 0.01-inch inner diameter Teflon tubing (Fig. 1).

The flow of solution through the XAS-SEC cell was achieved using a reciprocating pair of syringes driven by the same pulse train but having their direction of travel reversed.

In order to maximize contact of the solution with the WE and to minimize the net consumption of the sample a pulsed flow pattern was applied during electrochemical reactions and throughout the collection of XAS spectra. An example of a 41:40 pulse pattern is shown in Fig. 2, where this involves the forward flow of solution corresponding to 41 stepper motor (SM) pulses followed by the backflow of solution by 40 SM pulses to complete the cycle. For each change in direction there is a deceleration and acceleration programmed so as to minimize the mechanical stress on the SM. For the 1 ml syringe and SM/lead screw combination pump used for the experiment, 24 stepper motor pulses were required to displace 1  $\mu$ L of solution; conse-

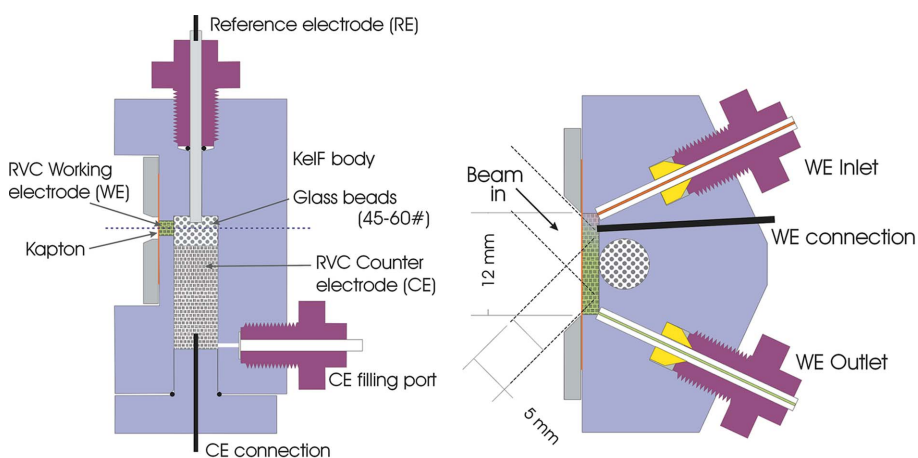


**Figure 1**

Vertical (left) and horizontal (right) sections through the working electrode chamber of the fluorescence X-ray absorption spectroscopy spectroelectrochemical (XAS-SEC) cell. The control of solution flow is achieved using syringe pumps and 1/16-inch Teflon tubing. The inlet and outlet tubes of the WE are sealed with the aid of Teflon ferrules; a flanged seal was used for the CE tubing.

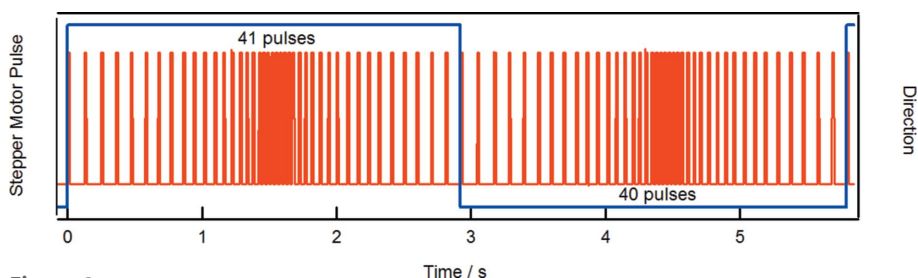


**Figure 2**

Stepper motor pulse profile used for a single cycle for a 41:40 pulse flow experiment. The solution flow is ramped with each change of direction. For a 1 ml syringe this gives a forward flow of 1.667  $\mu\text{L}$  and reverse flow of 1.625  $\mu\text{L}$  in each cycle.

quently a net flow of 1 SM pulse per cycle corresponds to a net solution flow of 26  $\mu\text{L h}^{-1}$ . The net flow depends on the number of back steps, the differential between the number of forward and back steps, slew rate and the acceleration/deceleration ramp, where each is able to be adjusted so as to minimize the effects of both photoreduction and disturbance of the solution.

### 2.3. Beamline and equipment

**2.3.1. Equipment.** Teflon tubing and fittings (Alltech) were used in conjunction with Hamilton HV valves and Hamilton gas-tight syringes to enable solution flow to the XAS-SEC cell. The stepper motor syringes were built in the workshop of the University of Melbourne and controlled using CNC CAT TB6560 stepper motor driver board interfaced to the printer port of a PC. In-house programs were developed for controlling the stepper motors.

A PAR model 363 potentiostat was controlled using either an eDAQ e-corder 207 interface and Chart (AD Instruments) software or a NI interface (BNC-2090A) integrated into the EPICS experiment control software. XAS experiments were recorded after the initial exponential current change was complete (typically 1–2 min). Typical current decay plots are shown in Fig. 3(b). An important diagnostic of the state of the sample is the stability of the current response during XAS data collection. For the pulsed-flow pattern used for the experiment, the current response depends on the solute concentration and the net flow rate. The current response for XAS collection from trioxalatoferrate(II) is shown in Fig. 3(d). In cases where the sample flow through the electrode is disturbed by the formation of gas bubbles or the build-up of decomposition products, the current response becomes irregular (e.g. Fig. 3e).

**2.3.2. Beamline.** Iron *K*-edge XAS experiments were performed at the wiggler XAS beamline at the Australian Synchrotron (Glover *et al.*, 2007). The storage ring operated at 3.0 GeV in top-up mode (200 mA). The incident photon energy was controlled using a cryogenically cooled Si(111) double-crystal monochromator, operated at the top of the rocking curve ('fully tuned'). Higher-order harmonics were rejected using an upstream vertically collimating mirror (Si), and a downstream toroidal focusing mirror (Rh). The energy scale was calibrated using an Fe metal foil as an internal

standard with the first inflection point,  $E_0$ , set to 7110.75 eV (Kraft *et al.*, 1996).

XAS were typically collected between 6914 and 7974 eV (6914–7093 eV, 8 eV step, 2 s; 7093–7163 eV, 0.25 eV step, 2 s; above 7163 eV, step size approximately constant in  $k$ , increasing count time from 2 to 10 s) in fluorescence mode using a 100 pixel HP-Ge detector (Canberra). The 100 individual channels were normalized using the freeware *Sakura* (Kappen *et al.*, 2015).

Calibration, averaging of multiple measurements and normalization of XANES data were performed using the *XFit* software package (Ellis & Freeman, 1995). The spectra were normalized (using the *Spline* program within the *XFit* package) according to the method of Penner-Hahn and co-workers (Weng *et al.*, 2005) to match the tabulated X-ray cross-section data (Hubbell *et al.*, 1974, 1975) for Fe [in a similar manner to the earlier work on Cr(III) XANES spectra] (Nguyen *et al.*, 2008).

### 3. Results and discussion

A key element of the strategy underpinning the XAS-SEC cell design is the pulse-flow pattern of solution in the WE. This both maximizes contact between the solute and the WE (Yeo *et al.*, 2012) and can minimize the impact of photoreduction while maintaining efficient use of the sample. The utility of the approach is demonstrated by experiments conducted on

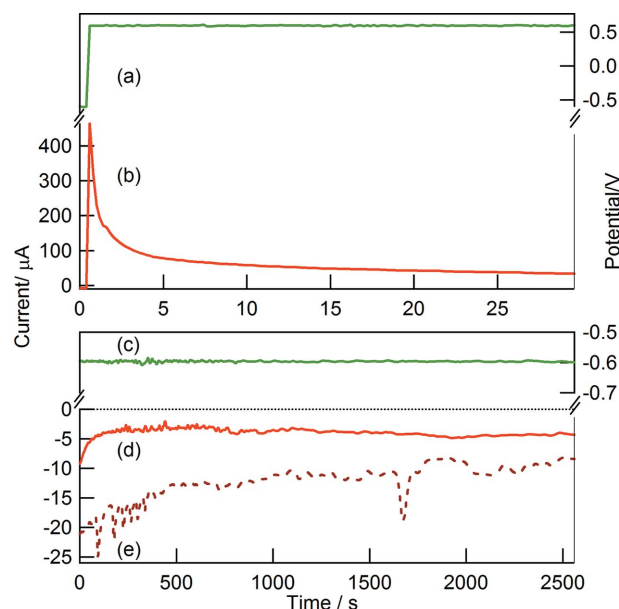


**Figure 3**

Applied potential and current response from the XAS-SEC cell of a 15 mM solution of  $\text{K}_3[\text{Fe}(\text{ox})_3]$  in aqueous KCl (0.2 M) subject to a 41:40 pulse flow; (a, b) immediately following the application of an oxidizing potential to a reduced sample; (c, d) during the collection of the XAS spectra. Trace (e) shows the current response for a sample where gas bubbles had formed in the WE compartment.

solutions of  $\text{K}_3[\text{Fe}(\text{ox})_3]$ , a well known chemical actinometer (Baumann *et al.*, 1983; Fischer & Warneck, 1996; Krishnaan *et al.*, 1981). Photoexcitation leads to  $\text{Fe}^{\text{III}}$  reduction and the oxidation of oxalate to  $\text{CO}_2$ . Spectra recorded from the XAS-SEC cell for static and pulsed solutions of  $\text{K}_3[\text{Fe}(\text{ox})_3]$  are shown in Fig. 4. For the static solution there was poor reproducibility of the XAS which was manifest by an offset in the fluorescence intensity, the magnitude of which was not constant across the spectrum (Fig. 4, green traces). At longer, and variable, times there was a catastrophic loss of fluorescence intensity and a change in profile of the spectrum (Fig. 4, pink traces) which was consistent with the formation of gas bubbles at the point of irradiation of the sample. The application of the 41:40 pulse sequence shown in Fig. 2 allowed the collection of spectra that were consistent with a well defined  $\text{Fe}^{\text{III}}$  species and with a high level of short- and long-term reproducibility of the spectra (Fig. 4, blue traces). The observed XANES matched closely that of the spectrum reported for intercalated  $[\text{Fe}(\text{ox})_3]^{3-}$  in  $\text{Mg}_2\text{Al}$  layered double hydroxide (Huang *et al.*, 2012). It is important to note that the pulsed flow leads to a steady state concentration of illuminated sample. If a  $2\text{ mm} \times 2\text{ mm}$  section of solution is considered to move back and forth with the pulsed flow, then the 41:40 pulse would correspond to a residence of 14 min in the  $1.5\text{ mm}$ -wide beam. Since the beam height ( $0.25\text{ mm}$ ) is less than the  $2\text{ mm}$  height of the sample slot, mixing would reduce the effective residence time by a factor of eight, this being further reduced when account is taken of the lowering of the beam intensity with depth into the sample. Thus, the 41:40 pulse flow would correspond to a steady state with the sample exposure to the X-ray beam equivalent to  $\sim 1\text{ min}$  of irradiation of a static sample. Further, the flow characteristics of the system can be easily modified to accommodate the photosensitivity of the sample.

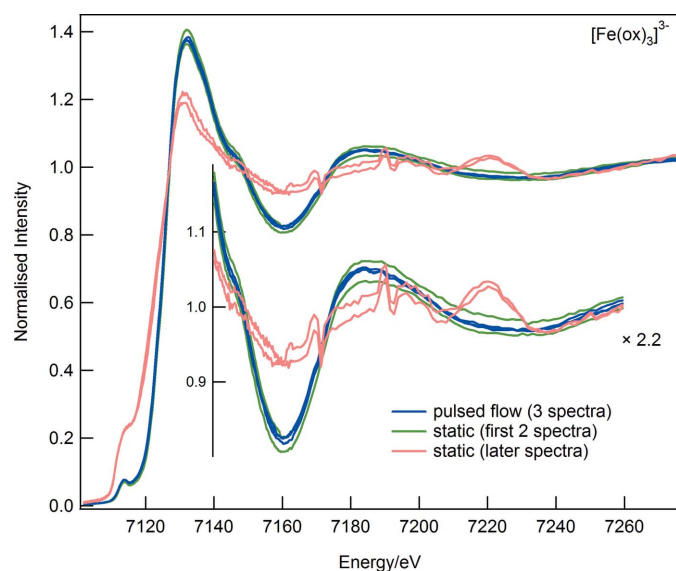


**Figure 4**  
Room-temperature ( $\sim 293\text{ K}$ ) XAS spectra of aqueous solutions of  $\text{K}_3[\text{Fe}(\text{ox})_3]$  ( $15\text{ mM}$ ) with  $0.2\text{ M}$  KCl from static solutions (green and pink) and solutions subject to a 41:40 pulse flow (blue, three spectra).

In addition to the spectra shown in Fig. 4, the impact of the pulsed flow on the background noise was assessed by monitoring time scans at constant energy. It was found that shorter higher-frequency pulses (*e.g.* 41:40 pulse) did not significantly increase the background noise while longer lower-frequency pulses (*e.g.* 500:490) introduced a sinusoidal component to the background signal.

While very stable results were generally obtained under pulsed flow conditions, some problems were also encountered due to the development of gas bubbles in the WE. This may be due to incomplete degassing of the solution, slow build-up of  $\text{CO}_2$  from photoreaction or possibly the diffusion of the He surrounding the sample through the Teflon tubing. The latter alternative is consistent with an increased incidence of bubble formation with larger inner diameter Teflon tubing. While He diffusion may be prevented by the use of higher-density tubing (PEEK, PEEKsil) the current room-temperature sample environment is too constricted to allow the use of less flexible tubing. Notwithstanding these issues, the current results demonstrate that the pulsed-flow method provides a very stable solution sample for XAS measurements. Most importantly, photodamage can be minimized while maintaining a very low net sample requirement ( $26\ \mu\text{L h}^{-1}$ ).

The electrochemical performance of the XAS-SEC cell is demonstrated by reduction of  $[\text{Fe}(\text{ox})_3]^{3-}$  at a potential of  $\sim 50\text{ mV}$  (*versus* normal hydrogen electrode), this being in a range close to that of heme proteins (Burgess, 1978). The application of a reducing potential of  $-400\text{ mV}$  to the WE immediately resulted in a strong current response that decayed to a steady-state current over a period of  $\sim 20\text{ s}$  (Fig. 3*b*). Recovery of the oxidized species was obtained by application of a potential of  $+0.4\text{ V}$  where the redox interconversion was complete in a similar time period. Associated with the electrochemical conversion between the  $[\text{Fe}(\text{ox})_3]^{3-/4-}$  species are changes in the XANES, which are consistent with quantitative conversion between the species in the WE (Fig. 5). While the XANES spectrum of an authentic sample of  $[\text{Fe}(\text{ox})_3]^{4-}$  appears not to have been published previously, the changes in the pre-edge features together with the sign and magnitude of the edge shift are consistent with that expected for  $\text{Fe}^{\text{II}}$  and  $\text{Fe}^{\text{III}}$  complexes and the general form of the spectra are consistent with that of  $\text{Fe}(\text{ox})\cdot 2\text{H}_2\text{O}$  (Fang *et al.*, 2012). This material has octahedral coordination of the  $\text{Fe}^{\text{II}}$  centre with a pair of *trans* water molecules with two oxalate ligands completing the coordination sphere. The oxalate ligands bridge adjacent Fe centres to give a linear chain structure (Yu *et al.*, 2006). Comparison can be made between the XANES of trioxalatometallate(III/II) complexes of Fe and those recently published for Co; the latter were recorded as solids dispersed in cellulose and measured at  $15\text{ K}$  (Best *et al.*, 2016) (Fig. 5). Owing to the difference in valence electron count, some spectral changes are expected on moving from Fe to Co; however, the  $\text{Fe}^{\text{II}}$  and  $\text{Co}^{\text{III}}$  complexes are isoelectronic with similar geometry. As such, they may otherwise be expected to exhibit similar pre-edge features but this is not the case due to differences in spin state, with low-spin  $\text{Co}^{\text{III}}$  (Zarić & Niketić, 1991) and high-spin  $\text{Fe}^{\text{II}}$  (de S.

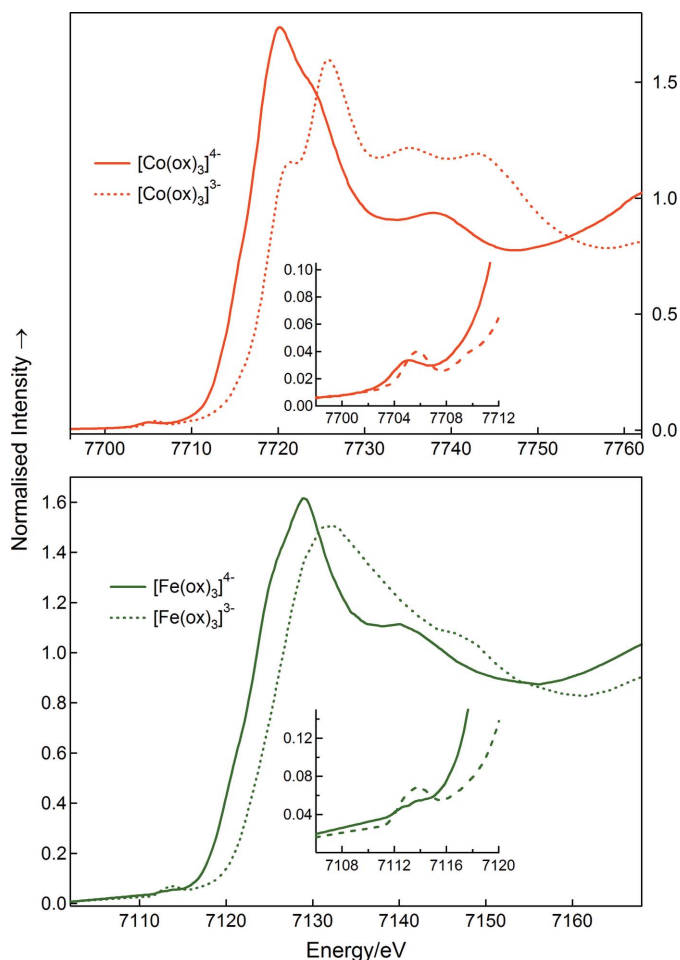


**Figure 5**  
Redox-state dependence of the XAS spectra of trioxalatometalate(III/II) complexes. Top:  $K_3[Co(ox)_3]$  and  $K_4[Co(ox)_3]$  dispersed in cellulose measured at 15 K (Best *et al.*, 2016). Bottom: room-temperature ( $\sim 293$  K) solution spectra of  $[Fe(ox)_3]^{3-}$  and  $[Fe(ox)_3]^{4-}$  obtained by *in situ* electrogeneration using the XAS-SEC cell.

Barros & Friedberg, 1966; Wendlandt & Simmons, 1966). For the low-spin,  $(t_{2g})^6$ , complex the pre-edge transitions will be of  $1s \rightarrow 3d$  ( $e_g$ ) character (7706 eV), which even with multiplet splitting gives a single feature. The high spin,  $(t_{2g})^4(e_g)^2$ , complex will have pre-edge transitions with both  $1s \rightarrow 3d$  ( $t_{2g}$ ) and  $1s \rightarrow 3d$  ( $e_g$ ) character and span a wider energy range (7112.5–7114.5 eV). Further, the simple one-electron reduction of  $[Fe(ox)_3]^{3-}$  in the XAS-SEC cell is clearly demonstrated by the similarity of the edge shift ( $\sim 2.5$  eV) of the trioxalatometalate(III/II) complexes of Fe and Co. It is significant that the transformation can be achieved with control over photolytic decomposition of the sample and with very modest sample requirements.

An important area of application for the XAS-SEC cell is the study of redox proteins, and the applicability of the approach to biomolecules is demonstrated by preliminary measurements conducted on the redox transport protein, cyt *c*. Spectra were measured from relatively concentrated protein samples (5 mM) and with 4,4'-bipyridine as the redox mediator (Eddowes & Hill, 1979). Spectral changes consistent with the reduction of the  $Fe^{III}$  form were observed immedi-

ately following the application of a reducing potential; however, reproducible spectra consistent with the fully reduced form required  $\sim 10$  min (Fig. 6a) to develop. The slow rate of electrogeneration is consistent with the low rate of heterogeneous electron transfer and this is reflected by the current response from the XAS-SEC cell (Fig. 6b). The stability of the current response during the collection of XAS is an important independent check of the stability of the sample and the state of the WE during the experiment.

The spectra of cyt *c* show a seemingly complicated set of potential-dependent spectral changes that are most straightforwardly interpreted using the pre-edge features. Prior to reduction, a broadened band at 7114 eV is observed (Fig. 6a), this being most consistent with low-spin ferricyt *c* (Cheng *et al.*, 1999; Giachini *et al.*, 2007). Reduction leads to broad pre-edge features near 7112.5 and 7114.5 eV reminiscent of high-spin  $[Fe(ox)_3]^{4-}$  and attributable to high-spin ferrocyt *c*. This is in contrast to measurements from samples at low temperatures (Cheng *et al.*, 1999; Giachini *et al.*, 2007) where a single sharp pre-edge feature near 7112 eV is observed and interpreted as due to a low-spin form. Reoxidation is not accompanied by the recovery of the initial spectrum, but is marked by a small shift of the bands to higher energy with an increase in intensity and decrease in the half-widths. These observations are typical of high-spin  $Fe^{II}$  and  $Fe^{III}$  proteins (Rich *et al.*, 1998) and suggest that oxidation leads to high-spin ferricyt *c*. The conversion of low-spin to high-spin ferricyt *c* by redox cycling through high-spin ferrocyt *c* has been previously reported based on surface-enhanced resonance Raman measurements (Hildebrandt & Stockburger, 1986), where the

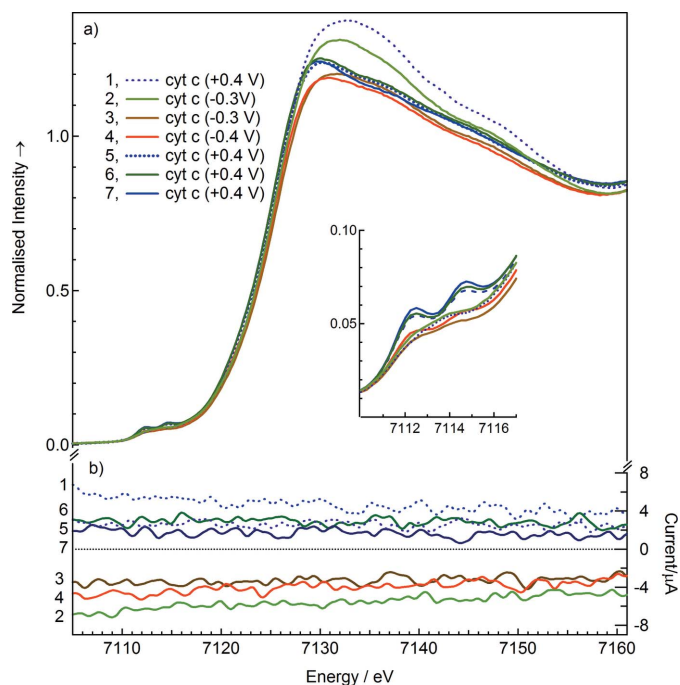


**Figure 6**  
XAS-SEC of cyt *c*. (a) XANES spectra recorded during a reduction/re-oxidation sequence. The spectra are labelled according to their order of measurement with the applied potential as indicated. (b) The current response recorded during the measurement of the spectra.

role of the Ag electrode in stabilization of the high-spin Fe<sup>III</sup> form a matter of speculation. The XAS-SEC measurements from cyt *c* suggest that similar behaviour occurs at a carbon electrode. A more detailed exploration of these effects requires further studies with more biologically relevant redox mediators and is beyond the scope of this manuscript. However, the current experiments demonstrate the importance of complementing cryogenic measurements with XAS spectra recorded under physiologically relevant conditions.

#### 4. Conclusions

Sampling strategies for the measurement of XAS spectra from solutions either in their resting or redox modulated states have been described. The approach allows the optimization of flow patterns so as to minimize beam damage while limiting the quantity of sample needed for the measurement of XAS spectra. The XAS-SEC cell in the pulsing mode allows rapid, controlled *in situ* electrosynthesis, and, when combined with rapid modes of data collection (Ginder-Vogel *et al.*, 2009; Zhang *et al.*, 2015) and advanced spectroscopic techniques (Chen *et al.*, 2014), will facilitate the study of reactive species generated at specific potentials under conditions of pH and ionic strength that match those relevant to the chemical or biochemical sample. These issues are particularly important to resolving the details of catalytic systems but can also impact significantly on measurements from environmental samples where beam damage constraints require that measurements be conducted at low temperatures. The low and efficient use of sample makes possible XAS structural investigation of the stable redox states of metalloproteins available only in ~1 mM concentration in 0.5–1 ml quantities.

#### Acknowledgements

SPB and PAL gratefully acknowledge the Australian Research Council for funding associated with this research (SPB: DP110101896; PAL: DP130103566 and DP140100176). Mr Marino Artuso is thanked for his skilled machining and input into the design of the XAS-SEC cell used in the work. This research was undertaken on the XAS beamline at the Australian Synchrotron, Victoria, Australia.

#### References

- Alonso, D. O. V., Dill, K. A. & Stigter, D. (1991). *Biopolymers*, **31**, 1631–1649.
- Bae, I. T., Tolmachev, Y., Mo, Y., Scherson, D., Scheidt, W. R., Ellison, M. K., Cheng, M. C., Armstrong, R. S. & Lay, P. A. (2001). *Inorg. Chem.* **40**, 3256–3258.
- de S. Barros, S. & Friedberg, S. A. (1966). *Phys. Rev.* **141**, 637–640.
- Baumann, H., Strehmel, B., Timpe, H. J. & Rehorek, D. (1983). *J. Prakt. Chem.* **325**, 753–763.
- Beattie, J. K. (1988). *Adv. Inorg. Chem.* **32**, 1–53.
- Best, S. P. & Cheah, M. H. (2010). *Radiat. Phys. Chem.* **79**, 185–194.
- Best, S. P., Kolev, S. D., Gabriel, J. R. P. & Cattrall, R. W. (2016). *J. Membr. Sci.* **497**, 377–386.
- Bond, A. M. & Scholz, F. (2010). *Electroanalytical Methods: Guide to Experiments and Applications*, 2nd Rev., extended ed. Greifswald: Springer.
- Bondin, M. I., Borg, S. J., Cheah, M.-H. & Best, S. P. (2006). *Radiat. Phys. Chem.* **75**, 1878–1883.
- Bondin, M. I., Borg, S. J., Cheah, M. H., Foran, G. & Best, S. P. (2006a). *Aust. J. Chem.* **59**, 263–272.
- Bondin, M. I., Foran, G. & Best, S. P. (2001). *Aust. J. Chem.* **54**, 705–709.
- Burgess, J. (1978). *Metal Ions in Solution*. New York: Wiley.
- Chapman, H. N. *et al.* (2011). *Nature (London)*, **470**, 73–77.
- Cheah, M. H. & Best, S. P. (2011). *Eur. J. Inorg. Chem.* **2011**, 1128–1137.
- Chen, L. X., Zhang, X. & Shelby, M. L. (2014). *Chem. Sci.* **5**, 4136–4152.
- Cheng, M. C., Rich, A. M., Armstrong, R. S., Ellis, P. J. & Lay, P. A. (1999). *Inorg. Chem.* **38**, 5703–5708.
- Craig, G. A., Roubeau, O. & Aromí, G. (2014). *Coord. Chem. Rev.* **269**, 13–31.
- Day, P., Smith, D. W. & Williams, R. J. P. (1967). *Biochemistry*, **6**, 1563–1566.
- Dewald, H. D., Watkins, J. W. II, Elder, R. C. & Heineman, W. R. (1986). *Anal. Chem.* **58**, 2968–2975.
- Dickson, C. F., Rich, A. M., D'Avigdor, W. M. H., Collins, D. A. T., Lowry, J. A., Mollan, T. L., Khandros, E., Olson, J. S., Weiss, M. J., Mackay, J. P., Lay, P. A. & Gell, D. A. (2013). *J. Biol. Chem.* **288**, 19986–20001.
- Eddowes, M. J. & Hill, H. A. O. (1979). *J. Am. Chem. Soc.* **101**, 4461–4464.
- Ellis, P. J. & Freeman, H. C. (1995). *J. Synchrotron Rad.* **2**, 190–195.
- Fang, L., Cao, Y., Huang, Q., Walker, S. L. & Cai, P. (2012). *Water Res.* **46**, 5613–5620.
- Feng, L., Gell, D. A., Zhou, S. P., Gu, L. C., Kong, Y., Li, J. Q., Hu, M., Yan, N., Lee, C., Rich, A. M., Armstrong, R. S., Lay, P. A., Gow, A. J., Weiss, M. J., Mackay, J. P. & Shi, Y. G. (2004). *Cell*, **119**, 629–640.
- Fischer, M. & Warneck, P. (1996). *J. Phys. Chem.* **100**, 15111–15117.
- George, G. N., Pickering, I. J., Pushie, M. J., Nienaber, K., Hackett, M. J., Ascone, I., Hedman, B., Hodgson, K. O., Aitken, J. B., Levina, A., Glover, C. & Lay, P. A. (2012). *J. Synchrotron Rad.* **19**, 875–886.
- Giachini, L., Francia, F., Cordone, L., Boscherini, F. & Venturoli, G. (2007). *Biophys. J.* **92**, 1350–1360.
- Ginder-Vogel, M., Landrot, G., Fischel, J. S. & Sparks, D. L. (2009). *Proc. Natl Acad. Sci. USA*, **106**, 16124–16128.
- Glover, C., McKinlay, J., Clift, M., Barg, B., Boldeman, J., Ridgway, M., Foran, G., Garret, R., Lay, P. & Broadbent, A. (2007). *AIP Conf. Proc.* **882**, 884–886.
- Guionneau, P. (2014). *Dalton Trans.* **43**, 382–393.
- Harris, D. & Loew, G. (1993). *J. Am. Chem. Soc.* **115**, 8775–8779.
- Hennig, C., Tutschku, J., Rossberg, A., Bernhard, G. & Scheinost, A. C. (2005). *Inorg. Chem.* **44**, 6655–6661.
- Hildebrandt, P. & Stockburger, M. (1986). *J. Phys. Chem.* **90**, 6017–6024.
- Huang, Z., Wu, P., Zhang, X., Wang, X., Zhu, N., Wu, J. & Li, P. (2012). *Appl. Clay Sci.* **65–66**, 87–94.
- Hubbell, J. H., McMaster, W. H., Del Grande, N. K. & Mallett, J. H. (1974). *X-ray Cross Sections and Attenuation Coefficients*, §2.1. in *International Tables for X-ray Crystallography*, Vol. 4, edited by J. A. Ibers & W. C. Hamilton, pp. 47–70. Birmingham: Kynoch Press.
- Hubbell, J. H., Veigele, W. J., Briggs, E. A., Brown, R. T., Cromer, D. T. & Howerton, R. J. (1975). *J. Phys. Chem. Ref. Data*, **4**, 471–538.
- Hutchens, T. W. & Yip, T. T. (1991). *J. Inorg. Biochem.* **42**, 105–118.
- Johansson, L. C. *et al.* (2012). *Nat. Methods*, **9**, 263–265.
- Kaim, W. & Klein, A. (2008). *Spectroelectrochemistry*. Cambridge: Royal Society of Chemistry.
- Kappen, P., Ruben, G. & Moll, A. (2015). *Sakura: a tool to pre-process fluorescence XAS data from multi-pixel detectors*, <http://www.synchrotron.org.au/aussynbeamlines/x-ray-absorption-spectroscopy/sakura>.

- Kraft, S., Stümpel, J., Becker, P. & Kuetgens, U. (1996). *Rev. Sci. Instrum.* **67**, 681–687.
- Krishnaan, G. U., Doshi, M. H. & Shah, A. B. (1981). *Radiochem. Radioanal. Lett.* **47**, 345–350.
- Levina, A., Armstrong, R. S. & Lay, P. A. (2005). *Coord. Chem. Rev.* **249**, 141–160.
- Levina, A., Foran, G. J., Pattison, D. I. & Lay, P. A. (2004). *Angew. Chem. Int. Ed.* **43**, 462–465.
- Levina, A., McLeod, A. I., Gasparini, S. J., Nguyen, A., De Silva, W. G. M., Aitken, J. B., Harris, H. H., Glover, C., Johannessen, B. & Lay, P. A. (2015). *Inorg. Chem.* **54**, 7753–7766.
- Levina, A., McLeod, A. I. & Lay, P. A. (2014). *Chem. Eur. J.* **20**, 12056–12060.
- Malati, M. A. (1999). *Experimental Inorganic/Physical Chemistry*, 1st ed. Chichester: Horwood.
- McBreen, J., O'Grady, W. E., Pandya, K. I., Hoffman, R. W. & Sayers, D. E. (1987). *Langmuir*, **3**, 428–433.
- Milsmann, C., Levina, A., Harris, H. H., Foran, G. J., Turner, P. & Lay, P. A. (2006). *Inorg. Chem.* **45**, 4743–4754.
- Nakamura, M. & Takahashi, M. (2013). *Mössbauer Spectroscopy: Applications in Chemistry, Biology, and Nanotechnology*, ch. 10, pp. 177–201. John Wiley and Sons.
- Nakanishi, K., Kato, D., Arai, H., Tanida, H., Mori, T., Orikasa, Y., Uchimoto, Y., Ohta, T. & Ogumi, Z. (2014). *Rev. Sci. Instrum.* **85**, 084103.
- Nguyen, A., Mulyani, I., Levina, A. & Lay, P. A. (2008). *Inorg. Chem.* **47**, 4299–4309.
- Nihei, M., Shiga, T., Maeda, Y. & Oshio, H. (2007). *Coord. Chem. Rev.* **251**, 2606–2621.
- Osheroff, N., Borden, D., Koppenol, W. H. & Margoliash, E. (1980). *J. Biol. Chem.* **255**, 1689–1697.
- Permien, S., Indris, S., Schürmann, U., Kienle, L., Zander, S., Doyle, S. & Bensch, W. (2016). *Chem. Mater.* **28**, 434–444.
- Rich, A. M., Armstrong, R. S., Ellis, P. J., Freeman, H. C. & Lay, P. A. (1998). *Inorg. Chem.* **37**, 5743–5753.
- Takao, K., Takao, S., Scheinost, A. C., Bernhard, G. & Hennig, C. (2010). *Inorg. Chim. Acta*, **363**, 802–806.
- Wachs, I. E. (2003). *Catal. Commun.* **4**, 567–570.
- Weckhuysen, B. M. (2003). *Phys. Chem. Chem. Phys.* **5**, 4351–4360.
- Wendlandt, W. W. & Simmons, E. L. (1966). *J. Inorg. Nucl. Chem.* **28**, 2420–2422.
- Weng, T.-C., Waldo, G. S. & Penner-Hahn, J. E. (2005). *J. Synchrotron Rad.* **12**, 506–510.
- Wiltshire, R. J. K., Smila-Castro, O., Connelly, N. G., Matthews, S. M., Fisher, A. C. & Rayment, T. (2009). *J. Phys. Chem. C*, **113**, 308–315.
- Yeo, J., Cheah, M. H., Bondin, M. I. & Best, S. P. (2012). *Aust. J. Chem.* **65**, 241–253.
- Yu, J.-H., Hou, Q., Bi, M.-H., Lü, Z., Zhang, X., Qu, X.-J., Lu, J. & Xu, J.-Q. (2006). *J. Mol. Struct.* **800**, 69–73.
- Zarić, S. & Niketić, S. R. (1991). *Polyhedron*, **10**, 2665–2672.
- Zhang, X., Lawson Daku, M. L., Zhang, J., Suarez-Alcantara, K., Jennings, G., Kurtz, C. A. & Canton, S. E. (2015). *J. Phys. Chem. C*, **119**, 3312–3321.